南京航空航天大学

论文集

（二〇一〇年） 第20册

电子信息工程学院

（第1分册）

电子信息工程学院

041

电子信息工程学院2010年发表论文目录

序号	姓名	单位	职称	论文题目	刊物、会议名称	发表时间	类别
1	李苗 崔铁军	041 041	副高 教授	High Frequency Methods for Simulation of High Resolution Imaging in Terahertz Regime	J Infrared Milli Terahz Waves	2010年31卷	
2	刘苗洪	041 041 041	博士 中级 教授	Three-level dual buck inverter with coupled-inductance	Asia-Pacific Power and Energy Engineering Conference	2010.3.28-31	
3	洪峰 稽鼎	041 041 041	中级 中级 教授	模拟光伏并网实验装置的研制	实验室研究与探索	2010年29卷8期	
4	陈春 柳 洪峰 王成	041 041 041 041	硕士 中级 教授 硕士	基于双buck逆变器光伏发电系统的稳定性研究	电气与能源工程学术会议论文集	2010.9.11	
5	王长 仟 郁斌 王成	041 041 041 041	硕士 中级 教授 硕士	The Design of Passive Intermodulation Reflected Test Instrument for GSM System	The 2010 International Congress on Computer Applications and Computational Science(CACS 2010)	2010.12.4-6	
6	欧阳静 王成	041 041 041	硕士 教授 中级	A Variable Step Maximum Power Point Tracking Method Using Taylor Mean Value Theorem	Asia-Pacific Power and Energy Engineering Conference	2010.3.28-31	
7	刘智 王成 华 王心	041 041 041 041	硕士 教授 硕士 硕士	The Design of Portable Transmitted PIM Test System Used in WCDMA System	The 2010 International Congress on Computer Applications and Computational Science(CACS 2010)	2010.12.4-6	
8	卜权 王成	041 041 041	硕士 教授 硕士	基于ARM9的嵌入式教学平台开发	电气电子教学学报	2010.10.15	
9	陈超 王心	041 041 041	硕士 硕士 教授	基于PSoC的实验教学平台开发	实验室研究与探索	2010.10.15	
10	杨伟 王成	041 041 041	硕士 教授 中级	A Novel Design Method of Single-phase Inverter Controller Based on CPLD	APPEEC2010	2010.3.28	
11	郑颛 王成	041 041 041	硕士 教授 中级	基于快速有效值算法的逆变器三环控制策略	解放军理工大学学报（自然科学版）	2010年4期	
12	张颖 吴	041 041 041	中级 教授 讲师	Test Data Compression for System-on-Chip Using Advanced Frequency-Directed Run-Length（AFDR）Codes	未来工业工程与应用国际学术会议（ICFIFA 2010）	2010	
13	张颖 吴 宁玉 方鹏	041 041 041 041 041	中级 教授 硕士 讲师 讲师	Fault-tolerant Schemes for NoC with a Network Monitor	2010 10th International Symposium on Communication and Information Technologies（ISCIT 2010）	2010	
14	龚牡 丹 郭荣 辉	041 041	硕士 副教授	A Novel Spectrum Utilization Method for Cognitive Radio Applications	ME DIACOM2010（2010 International Conference on Multimedia Communications）	2010	
15	曹群 生 赵芳	041 041 041	正高 硕士 硕士	Application of the MPSTD Algorithm for Waveguide Structures	IET Microw. Antennas &Propag	2010年4卷10期	
16	夏汉 刚 王	041 041 041	硕士 博士 教授	Grid-Cell Combination in 3D-FDTD Modeling of ELF Propagation of the Earth	ICMMT2010 会议论文集	2010年	

序号	姓名	代码	学位/职称	论文题目	发表刊物/会议名称	时间	备注
17	陈新蕾 曹群	041 041	硕士 教授	Analysis of characteristics of two-dimensional Runge-Kutta multiresolution time-domain scheme	Progress In Electromagnetics Research M	2010年13卷	
18	孙慧	041 041	硕士 教授	Wilkinson功分器小型化的研究	微系统技术发展研讨会	2010	
19	晏源 曹群	041 041	硕士 教授	Microwave Absorbing Properties of Sinuous Antenna Filled with Absorbing Material	IEEE Internation Conference on Ultra-Wideband（ICUWB）	2010	
20	虞菊花	041 041	硕士 教授	蛇形防护线降低非平行传输线中串扰的研究	微波学报	2010年26卷6期	
21	虞菊花	041 041	硕士 教授	高速差分微带与过孔结构的全波及电路分析和研究	中国电子科学研究院学报	2010年5卷1期	
22	喻先卫	041 041	硕士 教授	Analysis and Design of a Dual-Band Microstrip Antenna	ISSSE2010会议论文集	2010	
23	王毅 夏汉	041 041 041	博士 硕士 教授	Analysis of ELF attenuation rate using the geodesic FDTD algorithm	ICMMT2010 会议论文集	2010	
24	夏汉刚 王	041 041 041	硕士 博士 教授	ELF/SLF电磁波传播的FDTD和GIS结合建模与分析	微波学报	2010年26卷4期	
25	夏汉刚 王	041 041 041	硕士 博士 教授	Local High Resolution Technique in FDTD Modeling of ELF Propagation in the Earth-ionosphere Cavity	IEEE Antennas and Wireless Propagation Letters	2010年9卷	
26	宋晗 刘少斌	041 041	硕士 教授	A novel miniaturization Wilkinson power divider using complementary spiral resonators（CSRs）	The 12th IEEE International Conference on Communication Technology	2010	
27	孔祥鲲 刘少斌	041 041	博士 教授	Study on the Cut-Off Frequence of One-Dimensional Plasma Photonic Crystals	2010 International Symposium on Signals, Systems and Electronics（ISSSE）in Nanjing, China on September 17-20, 2010	2010	
28	田晓青 刘少斌	041 041	硕士 教授	Circularly Polarized Microstrip Antenna With Slots For Beidou（COMPASS）Navigation System	2010 International Symposium on Signals, Systems and Electronics（ISSSE）in Nanjing, China on September 17-20, 2010	2010	
29	孔祥鲲 刘少斌	041 041	博士 教授	Anomalous Refractive Indices of One-dimension Absorptive Plasma Photonic Crystal	2010 International Symposium on Signals, Systems and Electronics（ISSSE）in Nanjing, China on September 17-20, 2010	2010	
30	李春早 刘少斌	041 041	硕士 教授	Theoretical Studies on Propagation of Electromagnetic Wave in Preformed Narrowed Plasma Channel	2010 International Symposium on Signals, Systems and Electronics（ISSSE）in Nanjing, China on September 17-20, 2010	2010	
31	周良 刘少斌	041 041	博士 教授	Novel Compact Bow-Tie Slot Antenna for Ultra-Wideband Applications	2010 International Symposium on Signals, Systems and Electronics（ISSSE）in Nanjing, China on September 17-20, 2010	2010	

32	吴苏琴 刘少斌	041 041	硕士 教授	Coaxial Probe-fed Circularly Polarized Microstrip Antenna for BeiDou RDSS Applications	International Conference on Microwave and Millimeter Wave Technology（ICMMT 2010）May 8-11, 2010	2010	
33	戴钊阳 刘少斌	041 041	硕士 教授	Development and Investigation of Reconfigurable Plasma Antenna	International Conference on Microwave and Millimeter Wave Technology（ICMMT 2010）May 8-11, 2010	2010	
34	高楠 刘少斌	041 041	硕士 教授	Quadrifilar Helix Antenna With Mechanically Tunable Compact Geometry	International Conference on Microwave and Millimeter Wave Technology（ICMMT 2010）May 8-11, 2010	2010	
35	陈宇 刘少斌	041 041	硕士 教授	Broad-Band Space-Filling-Based Slot Antenna	International Conference on Microwave and Millimeter Wave Technology（ICMMT 2010）May 8-11, 2010	2010	
36	魏寅生 刘少斌	041 041	硕士 教授	A Compact CPW_Fed Microstrip Patch Antenna Combining Koch Boundary and Triangle Slot	International Conference on Microwave and Millimeter Wave Technology（ICMMT 2010）May 8-11, 2010	2010	
37	孔祥鲲 刘少斌	041 041	博士 教授	A novel tunable filter featuring defect mode of the TE wave from one-dimensional photonic crystals doped by magnetized plasma	Phys. Plasmas	2010年17卷103506-103505期	
38	王身云 刘少斌	041 041	博士 教授	Finite-difference time-domain studies of low-frequence stop band in superconductor-dielectric superlattice	Chinese Physics B	2010年19卷8期	
39	刘梅林 刘少	041 041	博士 教授	Adaptive Sparse Grid Method for RCS Estimation of Object with Uncertain Shape	IET Electronics Letters	2010年46卷12期	
40	周良 刘少	041 041	博士 教授	Dual-band circularly-polarised antenna based on complementary two turns spiral resonator	Electronics Letters	2010年46卷14期	
41	兰婧怡 戴婧 牛帅	041 041 041	硕士 硕士 副教授	弱稳定性的三维HIE-FDTD方法在微波谐振器中的仿真应用	第25届南京地区研究生通信年会	2010	
42	刘颖 鲍卓如	041 041 041 041	硕士 硕士 硕士 副教授	RBF无网格法分析静态电磁场问题	第25届南京地区研究生通信年会	2010	
43	谢娇 杨	041 041	硕士 副教授	Huyens subgrid technique for FDID analysis of EBG structure	IEEE International Conference on Ultra-Wideband	2010	
44	牛帅 杨阳	041 041	硕士 副教授	A weakly conditionally stable finite-difference time-domain method for simulation of resonant cavity	IEEE Internation Conference on Microwave and Millimeter Wave Technology	2010	
45	谢娇 杨阳	041 041	硕士 副教授	A kind of subgrid technique for FDTD analysis of electormagnetic problems	Asia-Pacific International Symposium on Electromagnetic Compatibility	2010	
46	谢娇 杨阳	041 041 041	硕士 副教授 教授	Huygens subgrid technique for FDID analysis of plasma problems	IEEE Internation Conference on Microwave and Millimeter Wave Technology	2010	

47	刘云寇文	041 041 041	中 教 教	级 授 授	A Tri-Band Bandpass Filter Realized Using Tri-Mode T-Shape Branches	Progress In Electromagnetics Research	2010年105卷	
48	王默然	041 041	硕 教	士 授	一种用于全球卫星定位系统的三频微带天线	微波学报	2010年26卷S1期	
49	袁家德	041 041	博 教	士 授	曲面微带天线电磁散射特性分析	系统工程与电子技术	2010年32卷11期	
50	顾晶晶	041 041	硕 教	士 授	利用奇异值分解快速计算单站RCS的算法	微波学报	2010年26卷2期	
51	郁超	041 041	硕 教	士 授	介质体电磁散射分析中的等效偶极矩法	微波学报	2010年26卷2期	
52	袁家德 顾长青	041 041	博 教	士 授	Electromagnetic Scattering by Arbitrarily Shaped Stratified Anisotropic Media Using the Equivalent Dipole Moment Method	International Journal of RF and Microwave Computer Aided Engineering	2010	
53	袁家德 顾长青	041 041	博 教	士 授	Electromagnetic Scattering by Arbitrarily Shaped PES Targets Coated with Anisotropic Media Using Equivalent Dipole-Moment Method	J Infrared Milli Terahz Waves	2010	
54	邓宏伟 赵永久 张	041 042 042 042 041	博 教 硕 硕 硕	士 授 士 士 士	Compact quintuple-mode stub-loaded resonator and UWB filter	IEEE Microwave and Wireless Components Letters	2010年20卷8期	
55	邓宏伟 赵永久 张学	041 042 042 042 041	博 教 硕 硕 硕	士 授 士 士 士	Compact wide upper-stopband BPF using open stub loaded dual-mode resonator	MICROWAVE AND OPTICAL TECHNOLOGY LETTERS	2010年52卷10期	
56	邓宏伟 赵永久 张学	041 042 042 042 041	博 教 硕 硕 博	士 授 士 士 士	Compact Wideband Bandpass Filter with Quadruple-Mode Stub-Loaded Resonator	Progress in Electromagnetics Research Letters	2010年17卷	
57	邓宏伟 赵永久 张学	041 042 042 042 041	博 教 硕 硕 博	士 授 士 士 士	Compact dual-mode open stub-loaded resonator and BPF	Progress in Electromagnetics Research Letters	2010年14卷	
58	邓宏伟 赵永久 张学	041 042 042 042 041	博 教 硕 硕 博	士 授 士 士 士	Compact quadruple-mode UWB bandpass filter using open stub loaded multiple-mode resonator	IEEE International Conference on Ultra-Wideband	2010.9	
59	邓宏伟 赵永久 张	041 042 042 042 041	博 教 硕 硕 博	士 授 士 士 士	A Dual-Band BPF with DSIR and TSIR	IET Electronics Letters	2010年46卷1期	
60	邓宏伟 赵永久 张学	041 042 042 042 041	博 教 硕 硕 硕	士 授 士 士 士	Compact quintuple-mode UWB bandpass filter with good out-of-band rejection	Progress in Electromagnetics Research Letters	2010年14卷	
61	王吉康 赵永久	042 042 042 042	硕 教 博 硕	士 授 士 士	A Miniaturized UWB BPF Based on Novel SCRLH Transmission Line Structure	Progress in Electromagnetics Research Letters	2010年19期	

	姓名	代码	职称	论文题目	刊物名称	发表时间	
62	张学顺 赵永久 邓宏	042 042 041 042 042	硕　士 教　授 博　士 硕　士 硕　士	High Selectivity dual-mode Bandpass filter with source-loaded coupling	Progress In Electromagnetics Research Letters	2010.18	
63	张学顺 邓宏伟 张璐	042 041 042 042 042	硕　士 博　士 硕　士 教　授 博　士	Compact dual-band BPF for GPS and WLAN with Two Dual-mode Stepped Impedance Resonators	Global Mobile Congress 2010	40452	
64	张璐 邓宏伟 赵永	042 041 042 041 042	硕　士 博　士 教　授 硕　士 硕　士	Compact quadruple-mode UWB bandpass filter using open stub loaded multiple-mode resonator	IEEE International Conference on Ultra-Wideband	2010.9	
65	张璐 邓宏伟 赵永久	042 041 042 042 041	硕　士 博　士 教　授 硕　士 硕　士	Cross-Coupled UWB Bandpass Filter with Dual-mode Stepped Impedance Resonator	International symposium on Signals, Systems and Electronics	2010.9	
66	孙全 赵伟 赵永	042 041 042 042 042	硕　士 博　士 教　授 硕　士 硕　士	A Calibration Technique of 4-Port Vector Network Analyzers with a General 12-Term Error Model	IEEE International Conference on Ultra-Wideband Proceedings	2010.9	
67	孙全 赵永久 强	042 042 042 042 042	硕　士 教　授 博　士 副教授 硕　士	A Planar Ultra-wideband Antenna with Dual Notched Bands Based on SCRLH Resonator	The International Conference on Microwave and Millimeter Wave Technology	2010.3	
68	赵伟 赵永久 邓宏伟	041 042 041 041 041	博　士 教　授 博　士 硕　士 硕　士	A Compact 4-Component 2-D Finite-Difference Frequency-Domain (FDFD) Method with Equivalent Surface Impedance Boundary Condition for Multilayer Metal-Coated Waveguide	南航学报英文版	2010年38卷12期	
69	赵伟 赵永	041 042 041	博　士 教　授 博　士	Calibration of the Three-Port VNA Using the General 6-Term Error Model	Journal of Electromagnetic Wave and Application	2010年24卷2-3期	
70	赵伟 赵永久 邓宏	041 042 041 042 042	博　士 教　授 博　士 硕　士 副教授	A Hybrid MM/Compact 2-D FDFD Method for Rectangular Ridged Waveguide Discontinuities	Process In Electromagnetics Research M	2010年38卷12期	
71	赵伟 赵永久 秦红	041 042 041 042 042	博　士 教　授 博　士 硕　士 博　士	利用引入开关补偿误差的8项误差模型校准二端口矢量网络分析仪	南航学报	2010年38卷12期	
72	赵伟 赵永久 秦红	041 042 041 042 042	博　士 教　授 博　士 博　士 副教授	Calibration Algorithm of the N-Port Vector Network Analyzer Using the General Node Equation	IET Science, Measurement& Technology	2010年4卷6期	
73	赵伟 赵永久 强	041 042 042 042 041	博　士 教　授 博　士 副教授 博　士	利用模式匹配与四分量二维频域有限差分混合算法分析复杂截面波导不连续性	电子学报	2010年38卷12期	

High Frequency Methods for Simulation of High Resolution Imaging in Terahertz Regime

Zhuo Li · Tie Jun Cui

Abstract High resolution imaging in the terahertz (THz) frequency range is investigated theoretically in this paper through the use of the high frequency methods in computational electromagnetics (CEM). Physical optics (PO), shooting and bouncing ray (SBR) and truncated-wedge incremental length diffraction coefficients (TW-ILDCs) methods are combined together to compute the scattered fields, which are then used to construct the inverse synthetic aperture radar (ISAR) images through two dimensional fast Fourier transform (2D-FFT). The corresponding ISAR images clearly show that high range and bearing resolution can be easily realized for THz carrier waves with broad bandwidth.

Keywords THz imaging · High frequency method · TW-ILDCs

1 Introductions

In the past decade, researchers and technicians around the world have paid much attention to the theoretical and experimental investigation of THz technology [1]. Most of them focus on THz wave production [2], detection [3], spectroscopy [4], communication, imaging [5] and so on. THz imaging is the most active one for its existent and potential applications, such as security sensing, quality control inspection, biomedical imaging, *etc*. Since the first raster scanning THz image was reported in 1995 [6], many THz imaging technologies have been developed and many imaging methods have been proposed on how to enhance the resolution. Far-field imaging techniques with resolutions close to the diffraction limit have been demonstrated on biological tissues and semiconductors [5, 7]. Subwavelength resolutions require near-field techniques or new materials. Resolutions down to $7\,\mu m$ were achieved using metallic subwavelength apertures [8, 9] or optically gated apertures [10, 11].

Z. Li (✉)
School of Information Science and Technology, Nanjing University of Aeronautics and Astronautics, Nanjing 210016, People's Republic of China
e-mail: lizhuo@nuaa.edu.cn

T. J. Cui
State Key Laboratory of Millimeter Waves, Southeast University, Nanjing 210096, People's Republic of China
e-mail: tjcui@seu.edu.cn

However, exact numerical computation and simulation of the THz waves transmission characteristics still impede further theoretical study of THz imaging. In the real world, many physical small objects cannot be regarded as electrical small ones as the frequency goes into THz regime. So the full wave analysis methods, such as the method of moments (MoM), the multi-level fast multiple algorithm (MLFMA) [12, 22] and the finite element method (FEM), which can be used to solve many electromagnetic (EM) problems precisely, become disabled for the prohibitively increasing memory requirements (MR) as well as computational complexity and time (CCT) [13–16]. Alternatively, high frequency (HF) methods, such as geometrical optics (GO), physical optics (PO), geometrical theory of diffraction (GTD), physical theory of diffraction (PTD), equivalent electric current (EEC) and incremental length diffraction coefficients (ILDCs) can be implemented to solve the HF problems asymptotically. And the higher the frequency is, the more accurate result of HF methods we can obtain. This is due to the fact that HF methods are based on the asymptotic expansions with respect to inverse powers of ω (or a large parameter proportional to ω) of solutions to boundary value problems for homogeneous or inhomogeneous Helmholtz's equation (or wave equation derived from Maxwell's equations) [17]. So in this work, HF methods including PO, SBR [18] and TW-ILDCs [19] are combined together in the numerical simulations and ISAR imaging in the THz frequency range. Small angle rotation imaging or the so called Range-Doppler imaging method is implemented to construct the ISAR image. Simulations show that high bearing and range resolution can be easily realized for THz carrier waves with broad bandwidth. In the following sections, HF frequency methods and imaging principle are first outlined, then the correctness and applicability of PO, SBR and TW-ILDCs to the scattering problem in THz frequency range are discussed and analytical models are built, finally some numerical results are given to verify our analysis and conclusions.

2 Principles

In the THz frequency range, an $1\,mm \times 1\,mm \times 1\,mm$ metallic cube must be regarded as an electrical large object whose EM feature could be computed in terms of MoM or MLFMA with high MR and CCT. When the cube' size changes to $1\,cm \times 1\,cm \times 1\,cm$, these so-called exact methods become disabled. But the HF methods can easily handle this kind of problems without losing much precision, which are commonly used in the analysis of electrical large EM scattering and radiation problems for its low MR and CCT. So in this article, PO, SBR and TW-ILDCs methods are employed for computing the EM scattered field of PEC targets.

As we know, the PO method is a well-known and widely used HF approximation technique for the calculation of EM field scattered from perfect electrical conducting (PEC) structures. It's essential idea is based on the assumption that the induced current density $\mathbf{J}_{PO}$ is only localized on the illuminated surface in connection with the incident magnetic field $\mathbf{H}$ in terms of the equation

$$\mathbf{J}_{PO}(\mathbf{r}) = 2\delta\widehat{\mathbf{n}} \times \mathbf{H}^{Incident}(\mathbf{r}), \tag{1}$$

where the coefficient δ accounts for the shadowing effects. If the point of observation $\mathbf{r}$ lies in the shadowed region δ must be set to zero. Otherwise δ equals 1. This implies that in practical applications the contributions from edges, corners and all mutual interactions such as multiple reflections are neglected. This kind of treatment evidently cuts off a lot of

memory requirement and running time as opposed to MoM and MLFMA. SBR technique is a combination of GO with multi-reflections and PO. It was first proposed by H. Ling [18] to calculate the backward RCS of structures with cavity and then extended to arbitrary complex scattering problems. Also the diffraction contribution of edges and creeping waves, which are very important for precision improvement in HF methods, are not considered in SBR. Among the wedge diffraction computation techniques, the TW-ILDCs method [19] is a high precision and robust one. During 2002–2004, the TW-ILDCs and the shadow boundary incremental length diffraction coefficients (SB-ILDCs) [20] method are both integrated in the SBR tracing code suited in Xpatch [21] to consider higher-order diffraction phenomena such as the creeping waves and the truncation effects due to the diffraction from finite sized wedge faces. For detailed formulas and manipulations of PO, SBR and TW-ILDCs, one can refer to Ref. [18, 19]. Then the small angle rotation imaging is implemented through small rotation of the incident plane wave to obtain high bearing resolution and broad bandwidth to obtain high range resolution. We remark that although we rotate the direction of the incident plane wave we can consider that the object is rotated instead because their relative position can be exchanged. As we know, when the rotation angle is small and the bandwidth is narrow, the imaging data can be approximated as a rectangular spectral window. In such circumstances, the two dimensional data are decoupled and the image can be constructed through 2D-FFT directly. When the rotation angle is large and the bandwidth is broad, the two dimensional data do not satisfy the decoupling condition. So the polar coordinate data must be first transformed to the rectangular coordinate form through interpolation and then used to construct images through 2D-FFT. In this paper, small angle rotation is assumed that the two dimensional data can be viewed as decoupled and the 2D-FFT is directly used to construct the final ISAR images. The transformation formula can be simplified as

$$\widetilde{f}(x,y) = \int_{\phi_{min}}^{\phi_{max}} \int_{k_{min}}^{k_{max}} kF(k,\phi) \exp[j2\pi k(y\cos\phi - x\sin\phi)]dkd\phi, \tag{2}$$

in which $F(k,\phi)$ is the radar echo information and θ is the rotation angle, k is the wavenumber in free space. ϕ_{min} and ϕ_{max} are the initial and final rotation angle respectively. k_{min} and k_{max} are the minimum and maximum wavenumber according to the scanning frequency from f_{min} to f_{max}. $k_{min} = 2\pi f_{min}/C$, $k_{max} = 2\pi f_{max}/C$. C is the velocity of light in free space. $\widetilde{f}(x,y)$ is the corresponding estimation value of the image. For this two fold integration we always transform it into progression and choose a series of angle and frequency sampling points to give an approximation, from which the ISAR image value can be finally obtained for each coordinate (x,y).

Now we briefly explain how these ISAR images are constructed and how these sampling points are chosen to make the whole image range accommodate the whole real object. If we denote the bearing resolution as $\delta_r = C/2B$, in which C is the velocity of light in the vacuum and $B = f_{max} - f_{min}$ is the transmission bandwidth. Also we can denote the range resolution as $\delta_c = \lambda/2\phi$, in which λ is the wavelength according to the scanning center frequency $f_c = (f_{max} + f_{min})/2$ and $\phi = \phi_{max} - \phi_{min}$ is the scanning angle range. Under normal circumstances, in order to make the image look more like the real target, the bearing and range resolution is assumed to be equal, that is $\delta_r = \delta_c = \delta$. And then we must choose the sampling points N in both the bearing and range direction according to the resolution δ and the actual maximum length L of the target or the whole scene being simulated. Actually, if $2^{x-1} < L/\delta \leq 2^x$, then $N=2^x$. For an example, if $\delta=0.1m$ and $L=10m$, than $x=7$
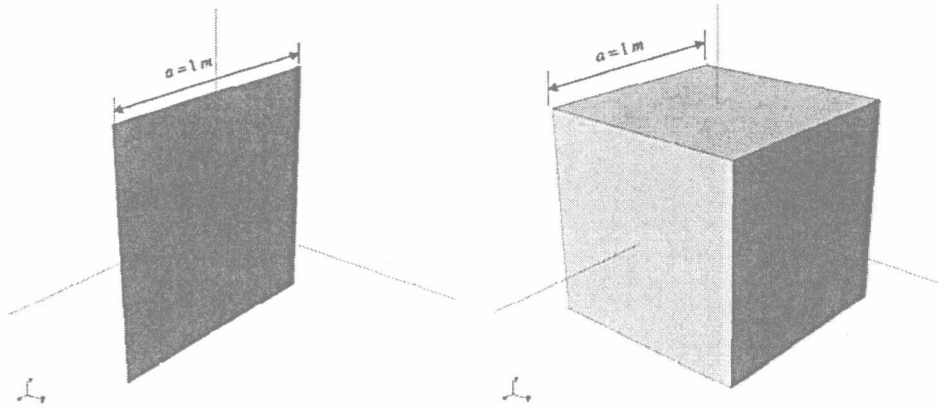
Fig. 1 The plate and cube model.

and $N = 2^7 = 128$. In addition, the radar echo information $F(k,\phi)$ of the whole target or scene is simulated for each sampling point according to different frequency f_i and angle ϕ_i, in which

$$f_i = f_{min} + \frac{f_{max} - f_{min}}{N - 1}(i - 1), \quad i = 1, \cdots, N \tag{3}$$

and

$$\phi_i = \phi_{min} + \frac{\phi_{max} - \phi_{min}}{N - 1}(i - 1), \quad i = 1, \cdots, N \tag{4}$$

Finally the ISAR images can be computed according to Eq. 2.

3 Simulations and analysis

First we compute the magnitude and phase of the electric field in the far field region of a plate and a cube shown in Fig. 1 in terms of PO/PO + TW-ILDCs compared with MLFMA

Fig. 2 The magnitude of the scattered electric field of a plate in the far field.
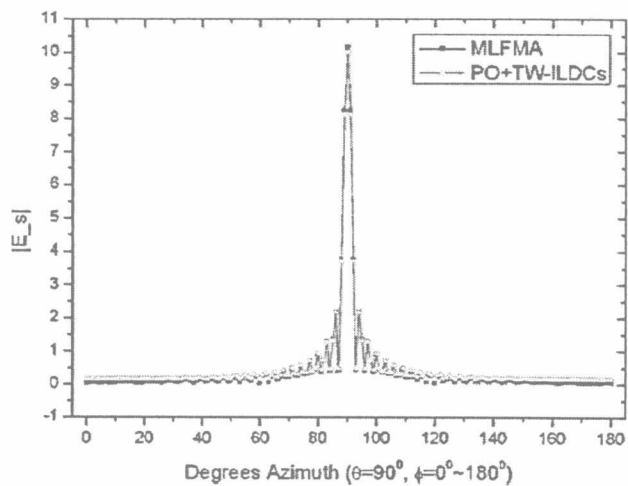
Fig. 3 The phase of the scattered electric field of a plate in the far field.
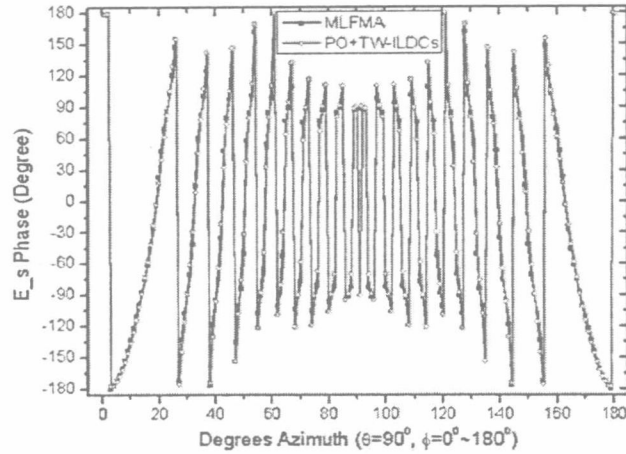
to verify that HF methods can be utilized for radar imaging simulations. For calculating both the magnitude and phase of the far field, we neglect the factor e^{-jkr}/r. The plate has the size of $1\,m \times 1\,m$ and the cube has the size of $1\,m \times 1\,m \times 1\,m$. The frequency is set as 3 GHz. The magnitude and phase are given in Fig. 2 (Fig. 4) and Fig. 3 (Fig. 5) respectively, which clearly show that the HF methods are effective and adequate in the EM field computation in the high frequency range. We also have verified in Ref. [23] that with the frequency goes into the THz regime, these so-called high frequency methods are still effective for simple PEC objects with flat planes.

These far field value including the amplitude and the phase are called the echo information, which can be used to construct the ISAR images through 2D-FFT. The generation of a two-dimensional (2-D) ISAR image can be constructed by plotting the intensity of the echoes as a function of frequency (that equates to the range) and angle. The term resolution refers to both the bearing resolution of the radar as determined by the object's rotation angle and the range resolution as determined by the transmitted bandwidth. The definition of high-resolution depends on the context, and in this instance is deemed to be the resolution that is required to identify natural and manmade features useful for autonomous applications. The THz signals,

**Fig. 4** The magnitude of the scattered electric field of a cube in the far field.
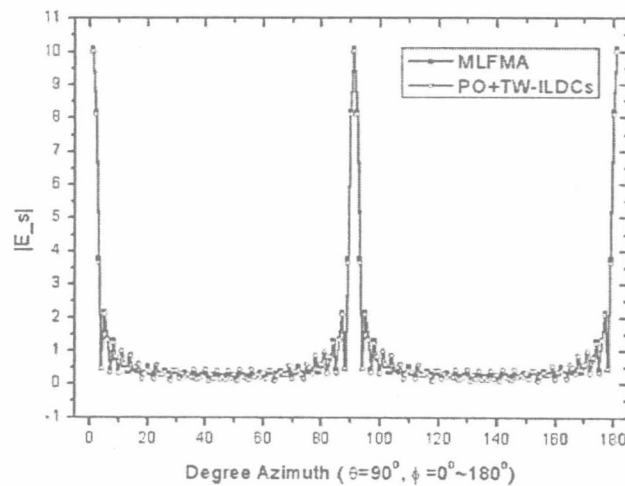
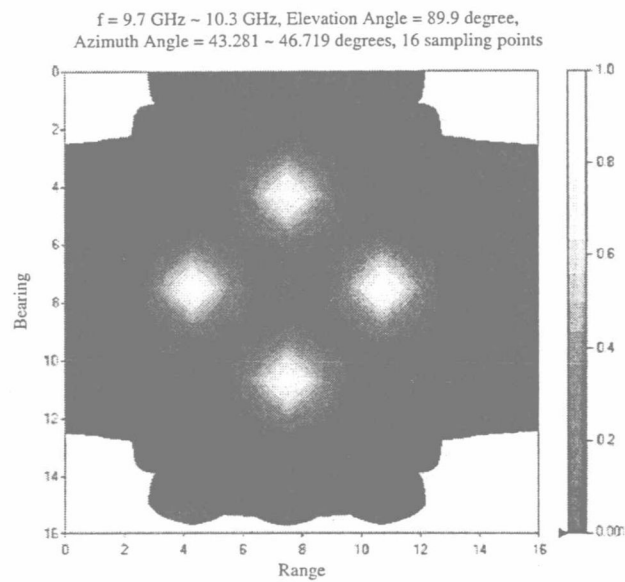Fig. 5 The phase of the scattered electric field of a cube in the far field.
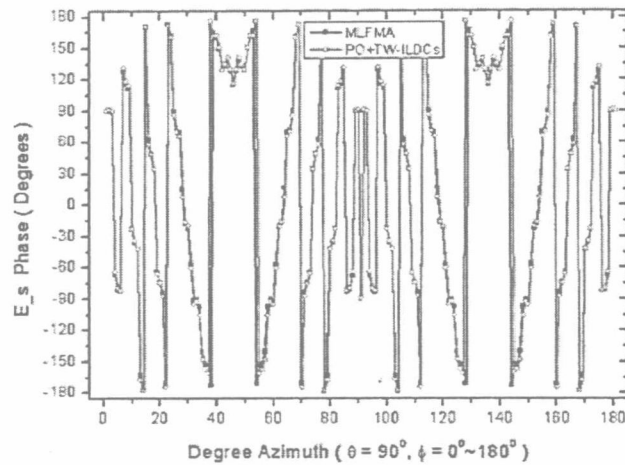
which have large transmission bandwidth, can be used to generate high-resolution ISAR images.

In order to illustrate the difference between GHz wave and THz wave, we first test a simple structure which has four $0.1\,m \times 0.1\,m$ rectangular plates with the distance of $1\,m$ shown in Fig. 6 and generate the ISAR images from GHz frequency range to THz frequency range in Figs. 7 and 8 respectively. The elevation angle is chosen as $\theta = 89.9°$ that the image can constructed from the plane perpendicular to the z axis. The azimuth angle starts from $\phi = 43.281°$ to $\phi = 46.719°$ in the GHz frequency range and from $\phi = 44.7°$ to $\phi = 45.3°$ in the THz frequency range to give a small rotation of the structure. The transmission bandwidth B is chosen as $B = 0.6$ GHz starting from 9.7 GHz to 10.3 GHz in the GHz frequency range and $B = 10$ GHz starting from 0.995 THz to 1.005 THz in the THz frequency range. The imaging results indicate that as the frequency rises and the bandwidth increases, the range resolution becomes higher and the four plates' corners can be clearly figured out. So from GHz to THz both the bearing and range resolution are enhanced.

Fig. 6 Four $0.1\,m \times 0.1\,m$ rectangular plates with the distance of $1\,m$.
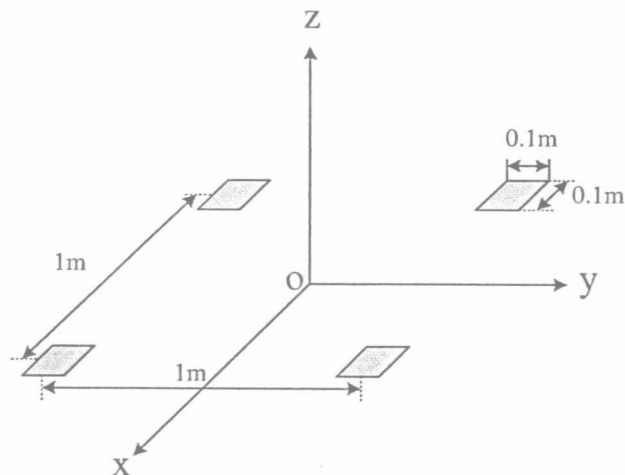
**Fig. 7** The ISAR image of the four plates structure in the GHz frequency range.

f = 9.7 GHz ~ 10.3 GHz, Elevation Angle = 89.9 degree, Azimuth Angle = 43.281 ~ 46.719 degrees, 16 sampling points
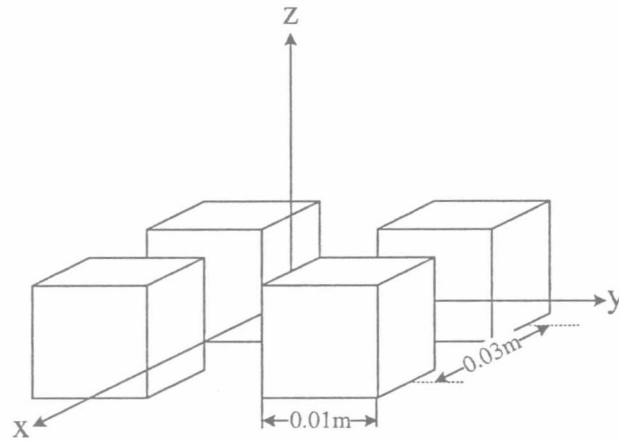
Then a more complex structure composed of four cubes is considered in Fig. 9 and SBR + TW-ILDCs method is chosen to calculate the scattered field for increasing the accuracy. Up to 3 time multi-reflections are considered in SBR for this complex structure and TW-ILDCs is implemented to compute the diffracted field. Finally these two fields are added together to give the total scattered field, which is then used to construct the ISAR image shown in Fig. 10. The elevation angle is chosen as $\theta=60°$ and the azimuth angle starts from $\phi=40.703°$ to $\phi=49.297°$. And the transmission bandwidth B is chosen as $B=150$ GHz starting from 0.925 THz to 1.075 THz that the relative bandwidth is further increased. For each cube there

Fig. 8 The ISAR image of the four plates structure in the THz frequency range.

f = 995 GHz ~ 1005 GHz, Elevation Angle = 89.9 degree, Azimuth Angle = 44.7 ~ 45.3 degrees, 256 sampling points
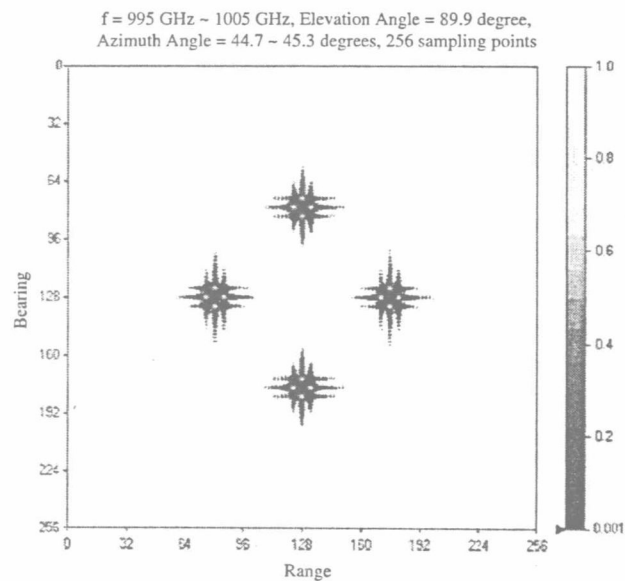
Fig. 9 Four $0.01\,m \times 0.01\,m \times 0.01\,m$ cubes with the distance of $0.03\,m$.
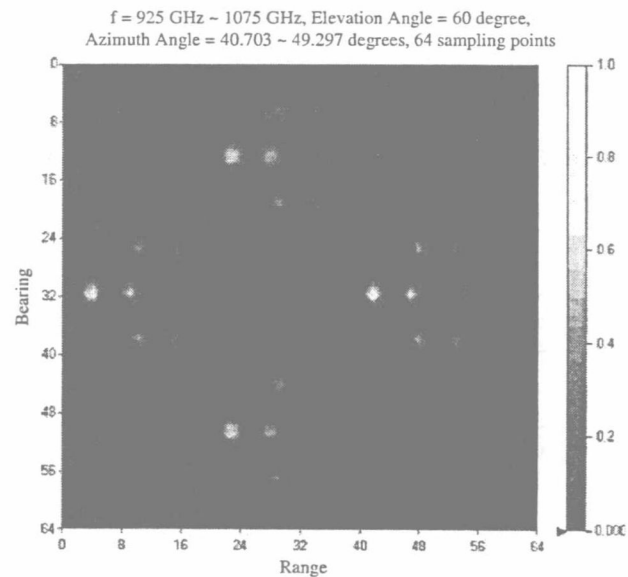

are seven bright points in the ISAR image, which indicate the cube's seven corners and strong scattering points. Only one point is lost for each cube in the image because this point is invisible to the incoming wave.

4 Conclusions

In this paper, the ISAR images of two 3D real targets in the THz frequency range are investigated via the HF methods. The reliability and correctness of the analysis have been verified by numerical results, from which we observe that a great enhancement of bearing and range resolution is obtained from GHz to THz frequency ranges. Hence we can fully use this high resolution in the target identification and detection.

Fig. 10 The ISAR image of the four cubes structure.

f = 925 GHz ~ 1075 GHz, Elevation Angle = 60 degree,
Azimuth Angle = 40.703 ~ 49.297 degrees, 64 sampling points

References

1. P. H. Siegel, "Terahertz technology," IEEE Trans. Microwave Theor. Tech. **50**, 910–928 (2002).
2. B. Ferguson and X. C. Zhang, "Materials for terahertz science and technology," Nat. Mater. **1**, 254801 (2002).
3. J. F. Federici, B. Schulkin, F. Huang, D. Gary, R. Barat, F. Oliveira, and D. Zimdars, "THz imaging and sensing for security applications-explosives, weapons and drugs," Semicond. Sci. Technol **20**, S266–S280 (2005).
4. M. C. Beard, G. M. Turner, and C. A. Schmuttenmaer, "Terahertz Spectroscopy," J. Phys. Chem. B **106** (29), 7146–7159 (2002).
5. H. T. Chen, R. Kersting, and G. C. Cho, "Terahertz imaging with nanometer resolution," Appl. Phys. Lett. **83**, 3009–3011 (2003).
6. B. B. Hu and M. C. Nuss, "Imaging with terahertz waves," Opt. Lett. **20** (16), 1716–1718 (1995).
7. P. Y. Han, G. C. Cho, and X. C. Zhang, "Time-domain transillumination of biological tissues with terahertz pulses," Opt. Lett. **250** (4), 242–244 (2000).
8. S. Hunsche, M. Koch, I. Brener, and M. C. Nuss, "THz near-field imaging," Opt. Commun. **150** (1), 22–26 (1998).
9. O. Mitrofanov, M. Lee, J. W. P. Hsu, I. Brener, R. Harel, J. F. Federici, J. D. Wynn, L. N. Pfeifer, and K. W. West, "Collection-Mode Near-Field Imaging With 0.5-THz Pulses," IEEE J. Sel. Top. Quantum Electron **7** (41), 600–607 (2001).
10. Q. Chen, Z. Jiang, G. X. Xu, and X. C. Zhang, "Near-field terahertz imaging with a dynamic aperture," Opt. Lett. **25** (15), 1122–1124 (2000).
11. N. C. J. van der Valk and P. C. M. Planken, "Electro-optic detection of subwavelength terahertz spot sizes in the near field of a metal tip," Appl. Phys. Lett. **81** (9), 1558–1560 (2002).
12. J. M. Song, C. C. Lu, and W. C. Chew, "Multilevel fast multipole algorithm for electromagnetic scattering by large complex objects," IEEE Trans. Antennas Propag. **45**, 1488–1493 (1997).
13. G. D. Martinis, T. Goyette, M. Coulombe, and J. Waldman, "A 1.56 THz Spot Scanning Radar Range for Fully Polarimetric W-Band Scale Model Measurements," *Proceedings of the 22nd Annual Symposium of the Antenna and Propagation*, 2000.
14. J. F. Zhang and T. J. Cui, "Subtle detection of target profiles using submillimeter waves," *2006 Joint 31st International Conference on Infrared and Millimeter Waves and 14th International Conference on Terahertz Electronics*, Shanghai, China, Sept. 18–22, 2006, p. 16.
15. J. Waldman, H. R. Fetterman, P. E. Duffy, T. G. Bryant, and P. E. Tannenwald, "Submillimeter model measurements and their applications to millimeter radar systems," in *Proceedings of the 4th International Conference on Infrared Near-Millimeter Waves*, Dec. 1979, pp. 49"C50.
16. M. J. Coulombe, T. Horgan, J. Waldman, G. Szatkowski, and W. Nixon, "A 524 GHz polarimetric compact range for scale model RCS measurements," in *Proceedings of Antenna Measurements and Techniques Association*, Monterey, CA, Oct. 1999.
17. V. M. Babič, V. S. Buldyrev, and E. F. Kuester, *Short-wavelength diffraction theory: asymptotic methods* (Springer, Berlin, 1991).
18. H. Ling, R. C. Chou, and S. W. Lee, "Shooting and bouncing rays: calculating the RCS of an arbitrarily shaped cavity," IEEE Trans. Antennas Propag. **37**, 194–205 (1989).
19. P. M. Johansen, "Uniform Physical Theory of Diffraction Equivalent Edge Current for Truncated Wedge Strips," IEEE Trans. Antennas Propag. **44**, 989–995 (1996).
20. R. A. Shore and A. D. Yaghjian, "Shadow boundary incremental length diffraction coefficients applied to scattering from 3-D bodies," IEEE Trans. Antennas Propag. **40**, 200–210 (2001).
21. J. G. Moore, A. D. Yaghjian, and R. A. Shore, "Shadow Boundary and Truncated Wedge ILDCs in Xpatch," *IEEE Antennas and Propagation Society International Symposium*, 2005.
22. M. L. Hastriter, "A study of MLFMA for large-scale scattering problems," Ph.D. Thesis of University of Illinois at Urbana-Champaign, 2003.
23. Z. Li, T. J. Cui, X. J. Zhong, Y. B. Tao, and H. Lin, "Electromagnetic Scattering Characteristics of PEC Targets in Terahertz Regime," IEEE Antennas Propag. Magazine **51**, 39–50 (2009).

Three-Level Dual Buck Inverter With Coupled-Inductance

Miao Liu , Feng Hong , Chenghua Wang

College of Information Science and Technology
Nanjing University of Aeronautics and Astronautics
Nanjing , China,210016
liumiao@nuaa.edu.cn , hongfeng@nuaa.edu.cn, chwang@nuaa.edu.cn

Abstract—**Dual Buck inverter (DBI) is a new topology with characteristics of high frequency and high efficiency. Just like half bridge inverter, the output voltage is a bipolar PWM waveform and voltage stress is high. To overcome these problems, a novel three-level dual Buck inverter, which has uni-polar PWM waveforms output and low voltage stress, is proposed. And the half load-cycle mode of DBI remains in the new inverter. However, it may lead to over-voltage when the inductor current is discontinuous. Thus, two inductors of the inverter are coupled together, and the bridge voltage can be clamped, and the size of magnetic component and filter is reduced simultaneously. The topology remains the characteristics of high efficiency and high reliability. Experimental result verifies the analysis described.**

Keywords-inverter; three- level;half bridge; integrated magnetics.

I. INTRODUCTION

Compared with the conventional bridge-inverter, DBI has special characteristics of no shoot-through problem and no reverse-recovery of the parasitic diode of the switch and realizes high frequency and high efficiency. There are many similarities between DBI and half bridge inverter. Bus voltage surpasses twice of the maximum of output voltage. The voltage stress of the device is high, the utilization rate of the direct voltage is low, and works at bipolar modulating mode and harmonic contents of the output voltage is high[1].Furthermore, too large volume of magnetic component still exists in DBI.

Recently, multilevel technology is greatly concerned and researched. Because of the limitation of the manufactory technology, voltage endurance is inadequate. For high-voltage converter, the power switch can be in series. However, due to the inconsistency of the parameters and the asynchrony of the power switches, it is difficult to achieve the balance of voltage and it also brings about over-voltage of power switches so as to lose reliability. Multilevel technology is a good method to solve the problem of the series of power switches and ensures the voltage stress of the power switches to clamp to the voltage of capacitor both in transient and steady stage. The three-level double buck half bridge inverter can change the output voltage of arm bridge into uni-polar voltage. All of these will be discussed in detail in the following.

II. THE NOVEL THREE-LEVEL DUAL BUCK INVERTER

The circuit topology of DBI is shown in Fig.1. DBI adopts half period work mode[2] [3]. During the positive half cycle, the circuit Buck 1 works ,which is composed by the power transistor VT_1, freewheel diode VD_1, filter inductance L_1 and filter capacitor C_f ;during the negative half cycle, the circuit Buck 2 works ,which is composed by the power transistor VT_2, freewheel diode VD_2,filter inductance L_2 and filter capacitor C_f. u_o is output voltage, i_L is inductor current: in the positive half cycle, it is i_{L1},the current of inductor L_1; in the negative half cycle , it is i_{L2} , the current of inductor L_2; u_A is the voltage of A, u_B is the voltage of B.The type waves are shown in fig.2(t=5ms/div).
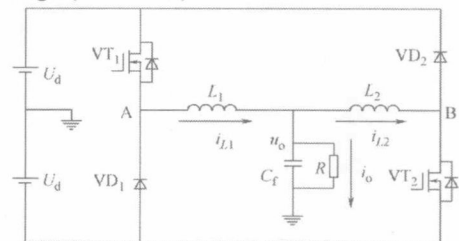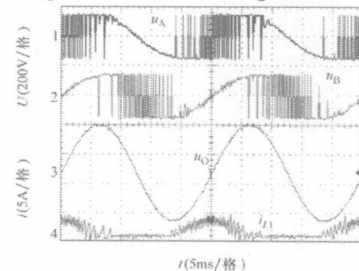

Fig.1 Dual Buck half bridge inverter

Fig.2 Typical waveforms of DBI

However the voltage stress of power switch of DBI is high, if the input direct bus voltage is $\pm U_d$, the voltage stress